

Hardness, yield strength, and plastic flow in thin film metallic-glass

J. C. Ye, J. P. Chu, Y. C. Chen, Q. Wang, and Y. Yang

Citation: *J. Appl. Phys.* **112**, 053516 (2012); doi: 10.1063/1.4750028

View online: <http://dx.doi.org/10.1063/1.4750028>

View Table of Contents: <http://jap.aip.org/resource/1/JAPIAU/v112/i5>

Published by the [American Institute of Physics](#).

Related Articles

Tensile and fatigue behaviors of printed Ag thin films on flexible substrates
Appl. Phys. Lett. **101**, 191907 (2012)

Lithiation-induced tensile stress and surface cracking in silicon thin film anode for rechargeable lithium battery
J. Appl. Phys. **112**, 093507 (2012)

Mechanical and thermal behaviors of nitrogen-doped Zr-Cu-Al-Ag-Ta—An alternative class of thin film metallic glass
Appl. Phys. Lett. **101**, 181902 (2012)

Effect of relative humidity on crack propagation in barrier films for flexible electronics
J. Appl. Phys. **112**, 083520 (2012)

Torsion fracture of carbon nanocoils
J. Appl. Phys. **112**, 084311 (2012)

Additional information on *J. Appl. Phys.*

Journal Homepage: <http://jap.aip.org/>

Journal Information: http://jap.aip.org/about/about_the_journal

Top downloads: http://jap.aip.org/features/most_downloaded

Information for Authors: <http://jap.aip.org/authors>

ADVERTISEMENT



Special Topic Section:
PHYSICS OF CANCER

Why cancer? Why physics? [View Articles Now](#)

Hardness, yield strength, and plastic flow in thin film metallic-glass

J. C. Ye,¹ J. P. Chu,² Y. C. Chen,^{1,2} Q. Wang,³ and Y. Yang^{1,4,a)}¹*Department of Mechanical Engineering, The Hong Kong Polytechnic University, Hung Hom, Kowloon, Hong Kong, People's Republic of China*²*Department of Materials Science and Engineering, National Taiwan University of Science and Technology, Taipei, 10607 Taiwan*³*Laboratory for Microstructures, Shanghai University, Shanghai 200072, People's Republic of China*⁴*Centre for Advanced Structural Materials, Department of Mechanical and Biomedical Engineering, City University of Hong Kong, Tat Chee Avenue, Kowloon Tung, Kowloon, Hong Kong, People's Republic of China*

(Received 30 May 2012; accepted 9 August 2012; published online 7 September 2012)

Thin film metallic-glasses (TFMGs) are a promising structural material for fabricating the next generation of micro- and nano-devices; however, a comprehensive study is still lacking today for understanding their mechanical behaviors. In this article, we present a systematic study on the $Zr_{53}Cu_{29}Al_{12}Ni_6$ TFMGs with varying thicknesses. Other than the intrinsic factor of structural amorphousness, our study pinpoints other extrinsic variables that could affect the hardness and yield strength of the TFMGs. Furthermore, the experimental results from microcompression show that the plastic flow in the TFMG-based micropillars exhibit strong sample size-and-shape dependence, which manifests as a smooth plastic deformation transition from the inhomogeneous to homogeneous mode when the TFMG-based micropillars with a submicron-scale film thickness are deformed into the shape of a low aspect ratio. © 2012 American Institute of Physics.

[<http://dx.doi.org/10.1063/1.4750028>]

I. INTRODUCTION

Metallic glasses (MGs), or amorphous metals, have a great potential as a structural material for future engineering applications. Owing to the lack of dislocation-like crystalline defects, MGs usually display a superb strength of 1–6 GPa,¹ much higher than their crystalline counterparts; however, the Achilles' heel of MGs is their apparent brittleness when deforming in a bulk form at room temperature (RT),² which is caused by the catastrophic growth of unhindered shear bands. In contrast, MGs in a small volume are considerably malleable even though shear-banding still dominates their post-yielding deformation.^{3–7} This plasticity “size effect” has recently stimulated intense research interest in the application of MGs to micro-electro-mechanical systems (MEMS).^{8–10} As the first attempt, MGs can be synthesized into thin films as a precursory form to make more complicated 3D microstructures,¹⁰ such that the high strength can be retained in the thin-film metallic-glasses (TFMGs) while brittle failure be avoided via size reduction.⁸ Despite the promise shown by the TFMGs in the structural applications of MEMS, however, to our best knowledge, there still lacks a systematic study aiming to provide a comprehensive understanding of the mechanical properties in TFMGs. Unlike MGs, TFMGs are generally bonded to a substrate. Therefore, when considering their mechanical behavior, one has to pay attention to a possible substrate effect, which may arise in a certain condition to couple with the aforementioned size effect. In such a case, a holistic view cannot be obtained with respect to the mechanical behavior of TFMGs until a systematic study has been performed. In the present work, we intend to characterize the

mechanical properties of a Zr-based TFMG with the focus on the combined substrate-and-size effect.

II. MATERIALS AND EXPERIMENTS

The $Zr_{53}Cu_{29}Al_{12}Ni_6$ (at. %) TFMGs with four thicknesses (400, 600, 800, and 1000 nm) were selected as the model material, which were deposited on a (100) silicon (Si) substrate via radio-frequency (RF) magnetron sputtering using a single target. As illustrated in Fig. 1, the Zr-Cu-Al-Ni alloy target was placed at the bottom side of the chamber, while the substrate was located on the top at a 10-cm working distance. In order to prevent undesirable chemical reactions, the base pressure of the chamber was maintained below 5×10^{-7} Torr before deposition. The working gas of Ar was subsequently introduced into the chamber at a flow rate of 20 sccm with the working pressure being controlled at 10 mTorr. During sputtering, it was detected that the chamber temperature could rise up to $\sim 80^\circ\text{C}$. After deposition, the TFMGs were cooled to the RT and taken out of the chamber for subsequent testing.

The basic nanomechanical properties of the TFMGs, including hardness and Young's modulus, were first obtained using the classic Berkovich nanoindentation approach, which were performed on the state-of-art nanoindentation system (TI950 HysitronTM TriboIndenter). Afterwards, focused-ion-beam (FIB) assisted micropillar compression tests were conducted to further reveal the possible size-and-substrate effect on the mechanical behavior of the TFMG-based micropillars. To this end, “composite” micropillar specimens, which consist of a TFMG top-layer and a Si under-layer, were milled out on the surfaces of the TFMG/Si samples using FIB. Owing to the ion-beam divergence, the FIBed micropillars are slightly tapered with a taper angle of $\sim 3^\circ$. The details of

^{a)}Author to whom correspondence should be addressed. Electronic mail: yonyang@cityu.edu.hk.

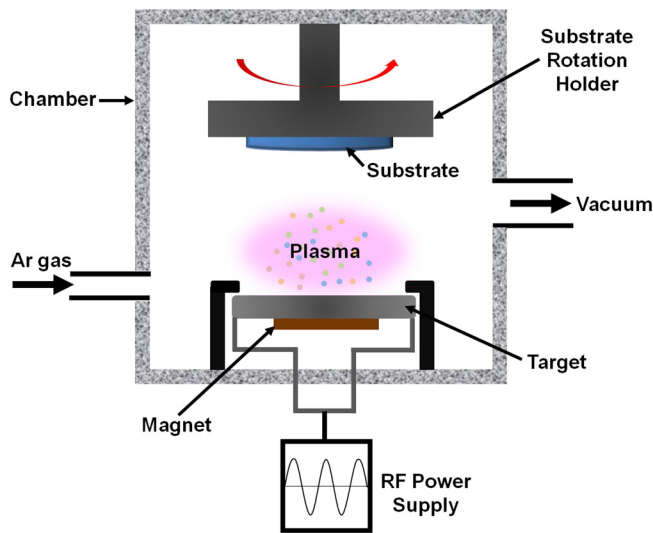


FIG. 1. The sketch of the RF magnetron sputtering system used for the deposition of TFMGs on a silicon substrate.

micropillar preparation are described elsewhere¹¹ and omitted here for brevity. After the FIB milling, the micro-compression tests were carried out at the nominal strain rate of $\sim 5 \times 10^{-3} \text{ s}^{-1}$ on the same HysitronTM nanoindentation system equipped with a $10 \mu\text{m}$ flat-end diamond tip. The morphologies of the micropillars before/after the micro-compression tests were subsequently imaged with the high-resolution scanning electron microscope (SEM, LEO 1530 Gemini, Zeiss, Oberkochen).

III. EXPERIMENTAL RESULTS

A. Structural characterization of TFMGs

The crystallographic characterization of the TFMGs was performed using a high-resolution grazing-incidence x-ray diffractometer (XRD, Bruker D8 Discover). The XRD results clearly indicate that these TFMGs are generally amorphous, as shown in Fig. 2. Further structural characterization

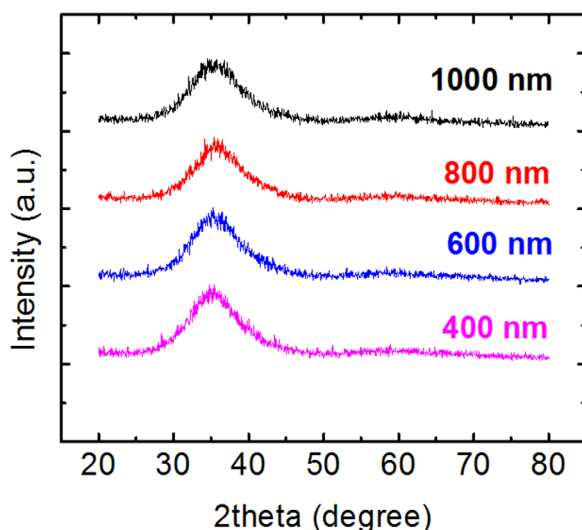


FIG. 2. XRD patterns of the Zr-based TFMG with various thicknesses ranging from 400 nm to 1000 nm.

was carried out by atomic force microscopy (AFM) (Bruker Multimode 8) to examine the surface topography of the TFMGs, and by high-resolution transmission electron microscopy (HRTEM) (Philips Tecnai G² F20) to confirm the structural amorphousness/crystallinity in selected local regions, such as the TFMG/Si interface region.

Regardless of the film thickness, the surface of the as-deposited TFMG looks quite smooth with the root-mean-square (RMS) roughness around $\sim 1 \text{ nm}$. However, with the increasing film thickness, it can be found that the surface roughness slightly increases from $\sim 0.8 \text{ nm}$ on the 400-nm film to $\sim 1.1 \text{ nm}$ on the 1000-nm film (Fig. 3(a)). The surface smoothness of the TFMGs can be also perceived at a much larger scale from the SEM micrograph (Fig. 3(b)), which validates the subsequent use of nanoindentation for measuring the nano-mechanical properties of the TFMGs. In contrast, the naturally exposed side face of the TFMGs appears relatively rough, exhibiting a columnar structure as seen in Fig. 3(b). Apart from these surface features, the atomic structure within the TFMG/Si interface region was imaged with the HRTEM technique. As shown in Fig. 3(c), it can be seen that there exists a 2-nm thick transition zone bridging the amorphous TFMG and the crystalline Si. On the basis of the image contrast, it may be inferred that the transition zone be made up of a native oxide layer (silicate). After the fast-Fourier-transform (FFT) filtering, the HRTEM image clearly reveals the variation of the atomic structure across the transition region. As seen in Fig. 3(d), the atomic structure displays an amorphous character at the side adjoining the TFMG whereas gradually adjusted to a crystalline setting with the increasing distance from the amorphous side.

B. Hardness of TFMGs

To measure the TFMGs' hardness, H_f and elastic modulus, E_f , a sequential nanoindentation approach was used, which utilizes the load function consisting of numerous loading/holding/unloading cycles (Fig. 4(a)). Following the Oliver-Pharr's (O-P) approach,¹² the apparent elastic modulus of the thin films was obtained after each load cycle, which, however, increases with the indentation depth, h , due to the substrate effect (see Fig. 12(a) in Ref. 13). By fitting the curves of E_f vs. h to the modified King's model¹⁴ with the Poisson's ratios of the TFMG and Si being taken, respectively, as 0.36 and 0.28, the intrinsic moduli of both TFMG and Si can be extracted simultaneously. Apart from that, the hardness of the TFMGs, which remains almost as a constant for the indentation depth falling below $\sim 10\%$ of the corresponding film thickness, was selected to be the material's intrinsic property.¹⁴ The set-up of the nanoindentation experiments and the related data analyses have been described in our recent review article.¹³ Interested readers may refer to Ref. 13 for further details.

As shown in Fig. 4(b), the Young's moduli of the TFMGs extracted using the modified King's model remains almost at constant ($\sim 117 \text{ GPa}$), which agree with the properties of the other Zr-based TFMGs already reported,¹⁵⁻¹⁷ and are also consistent with those of the Zr-based BMGs with a similar chemical composition. The Young's modulus of the

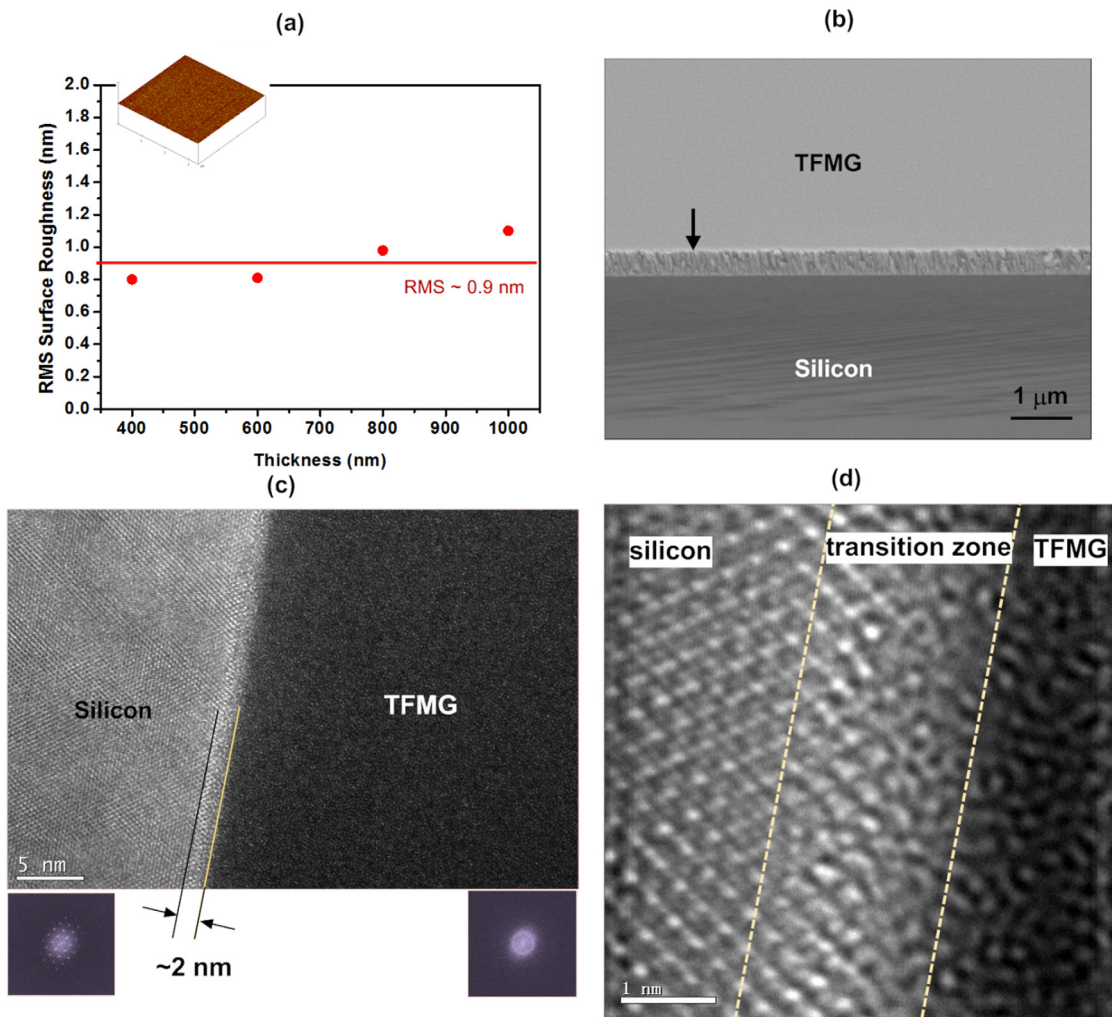


FIG. 3. (a) Variation of the RMS surface roughness characterized by AFM with the film thickness (inset shows the 3D perspective view of a TFMG surface), (b) the SEM micrograph showing the angle view of a 600-nm thick TFMG supported by a Si substrate (the arrow indicates where the cross section of the TFMG transitions to its top surface), (c) the HRTEM image of the TFMG bonded to the crystalline Si substrate with around 2-nm thick transition zone [insets are the typical FFT obtained from the corresponding TFMG and Si regions], and (d) the FFT-filtered HRTEM image revealing the structure of the transition zone bridging the amorphous and crystalline atomic structure.

Si substrate was found to be ~ 183 GPa, also in line with the literature results.¹³ However, we notice that the obtained hardness (~ 5.5 GPa) of the Zr-based TFMGs is unexpectedly low, about $\sim 20\%$ smaller than that (~ 6.2 GPa) of the corresponding Zr-based BMGs. We further find that this apparent film “softening” occurs not only to our Zr-based TFMGs but also to other TFMGs. To highlight this, the hardness-versus-modulus data obtained from different types of Zr-based TFMGs were plotted on the same graph with those of BMGs.^{18,19} As analogous to the known relation between the strength (σ_y) and Young’s modulus (E) of BMGs,²⁰ i.e., $\sigma_y = 0.02E$, the hardness vs. modulus data can be also fitted quite well to an empirical relation, i.e., $H = 0.069E$, across a wide range of modulus. As shown in Fig. 4(d), it can be found that the TFMG hardness is all below that of the BMGs with a similar modulus.

C. Microcompression

Based on our nanoindentation results, the hardness of the Zr-based TFMG (~ 5.5 GPa) is about half of that of the Si

substrate (~ 12.5 GPa). This implies that the microcompression could be used to supplement nanoindentation for further studying the mechanical behavior of the TFMGs. In this experimental setting, the Si substrate behaves at large as an elastic support. Furthermore, with the FIB micro-machining, we can fabricate the “composite” micropillars of different sizes and shapes, as shown in Figs. 5(a)–5(e). In doing so, we are enabled to tune the influence of the Si substrate on the yielding and post-yielding behaviors of the TFMGs by deliberately adjusting the ratio of film thickness, t_f , to pillar diameter, D , as will be seen in the later text.

1. Yield strength of TFMGs

From microcompression, the elastic moduli and yield strengths of the TFMGs can be measured. Figures 6(a)–6(d) display the typical load-displacement curves obtained from the micropillars of different sizes and shapes. By using the linear portion of these curves, a “composite” elastic modulus of the micropillar could be extracted after accounting for the tapering of the FIBed micropillar and the substrate

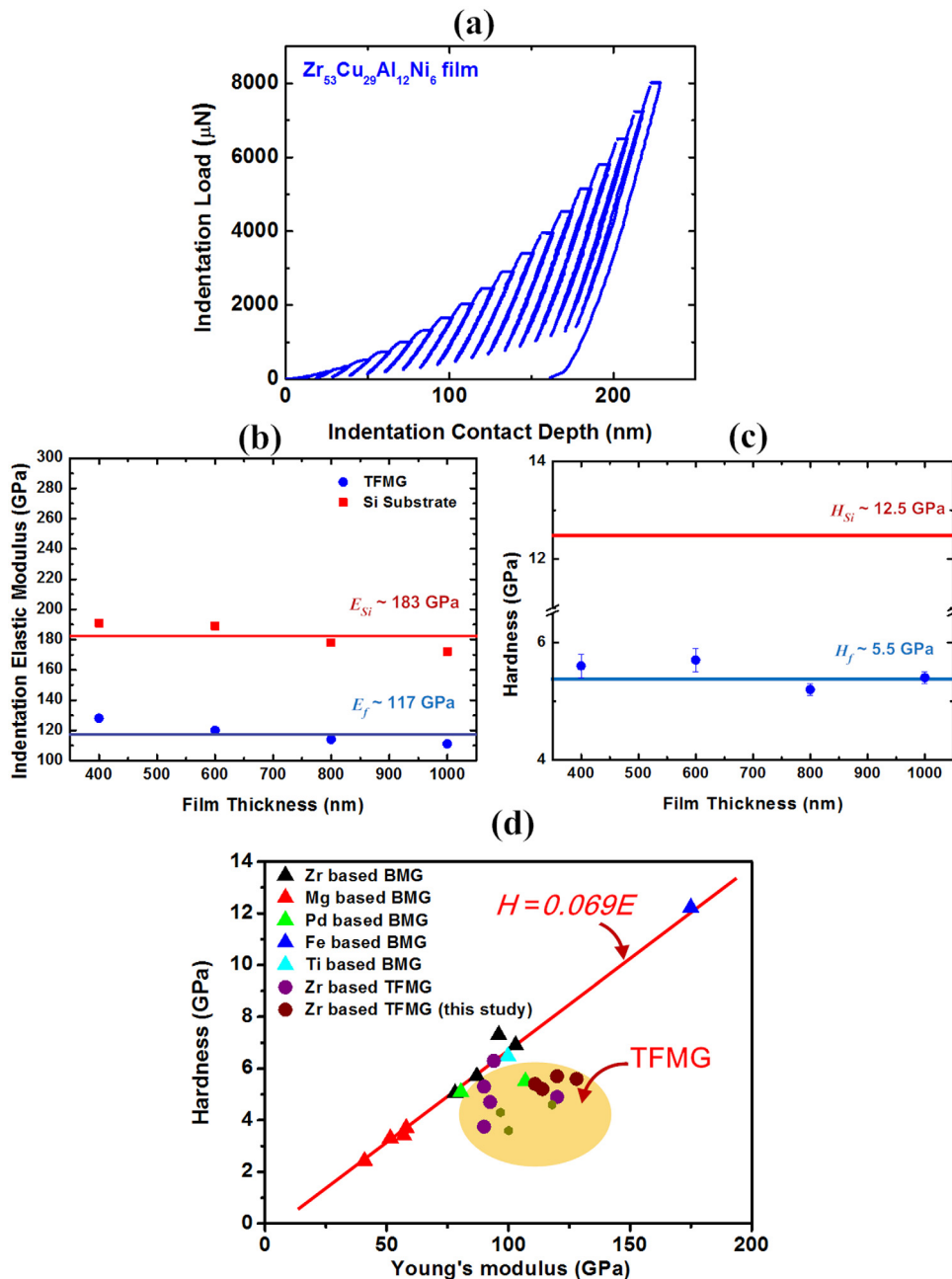


FIG. 4. (a) the typical load-displacement curve obtained from the TFMG/Si composite system in a sequential nanoindentation test, (b) the indentation elastic moduli of the TFMGs (E_f) and their underlying Si substrates (E_{Si}) extrapolated using the modified King's model,¹⁴ (c) the contact-depth-insensitive hardness of the TFMGs (H_f) and the pure Si substrate (H_{Si}), and (d) the comparison of the hardness-versus-modulus relation obtained from BMGs and TFMGs via indentation testing. The data of BMGs are adapted from Refs. 18 and 19 and those of TFMGs already reported from Refs. 15 and 17.

compliance¹¹ Subsequently, the elastic modulus of the TFMG top-layer can be obtained by subtracting the stiffness of the Si substrate out of the total stiffness of the micropillar. The details of the underlying mechanics have also been discussed in Ref. 13 and are thus omitted here as well. Following the already established method,¹³ the Young's moduli of the TFMGs were obtained, of which the average is ~ 108 GPa agreeing with the previous nanoindentation result.¹³

Since the Si under-layer is much stronger than the TFMG top-layer (Fig. 4(c)), the yield strengths, σ_y , of the TFMGs can be extracted directly from the load-displacement curves of the composite micropillars. By following the microcompression literature,²¹ we here treat σ_y as the nominal stress measure of P_y/A_0 , where P_y and A_0 denote, respectively, the yielding load and the cross sectional area of the micropillar at top.¹⁹ Figure 7(a) displays the yield strengths so obtained as a function the t_f/D ratio, from which it can be

inferred that, regardless of the film thickness, the yield strengths of the TFMGs can be viewed as a constant (~ 2.6 GPa) for $t_f/D > 0.5$; however, when $t_f/D < 0.5$, a substrate effect arises, leading to the increasing σ_y with the decreasing t_f/D ratio. Along the same line for the indentation hardness, the constant value of ~ 2.6 GPa was taken to be the intrinsic yield strength of the TFMG.

In Fig. 7(b), the data of σ_y vs. E obtained for the TFMGs are plotted together with those of the BMGs, from which it can be seen that all experimental data seemingly collapse onto the same master curve of $\sigma_y = E/50$. As H is known to be 2.8–3 times σ_y for a variety of MGs,¹⁹ the current finding strongly implies that the previous film softening, as revealed by the nanoindentation experiments, should stem from a tensile residual stress in the TFMGs, which facilitates yielding in the TFMGs bonded to a Si substrate, but is released after FIB milling and plays no role in microcompression.

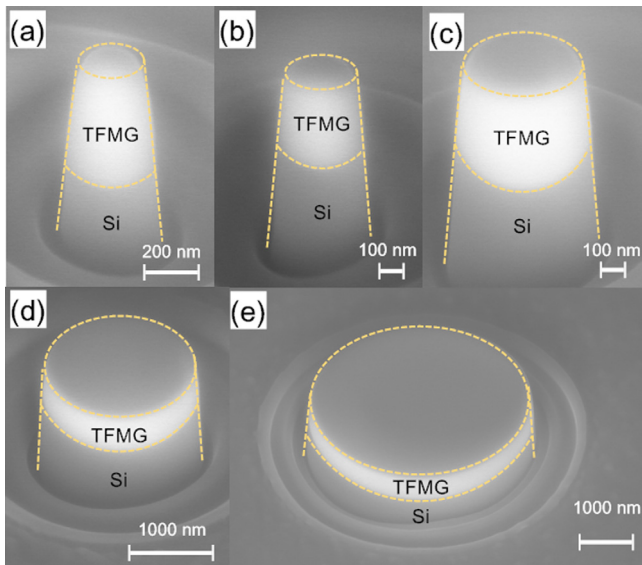


FIG. 5. (a)–(e) The SEM micrographs showing the TFMG/Si composite micropillars with different sizes and shapes. (Note that a sketched profile of the micropillar is superimposed on the corresponding SEM micrograph for clarity)

2. Post-yielding behavior of TFMGs

The post-yielding behavior of MGs under compression is usually characterized by a serrated load-displacement or pop-in response. Likewise, for a fixed film thickness, say, 600 nm,

pop-in was observed at the t_f/D ratio of 2.0 (Fig. 6(a)); however, no prominent pop-in could be found when the corresponding t_f/D ratio is reduced to 1.2, 0.3, and 0.1, as shown in Figs. 6(b) and 6(c). Given that the current nanoindentation system has a data acquisition rate of 10^4 s^{-1} , this behavior implies that the plastic flow appears temporally homogeneous at the time scale of $\sim 0.1 \text{ ms}$. After the microcompression tests, we examined the deformation morphologies of the micropillars using the high-resolution SEM. As shown by the insets of Figs. 6(a)–6(d), discernible shear banding can still be found on the deformed micropillars even though no prominent displacement pop-in is existent on the corresponding load-displacement curves. Furthermore, apparent work hardening could be observed in the micropillar with a low t_f/D ratio, or when the plastic flow in the micropillar with a large t_f/D ratio has progressed to a large extent.

IV. ANALYSES AND DISCUSSIONS

A. Residual stress

By comparing the microcompression to nanoindentation results, it is now sensible to conclude that the reduction in the TFMG hardness is caused by a tensile residual stress. With the pressure dependence of yielding in MGs, we here show that this residual stress can be quantified with ease. Assuming a residual-stress softened yield strength σ_0 , which is roughly one third of the nanoindentation hardness, the difference between the real strength, σ_y and the softened strength, σ_0 ,

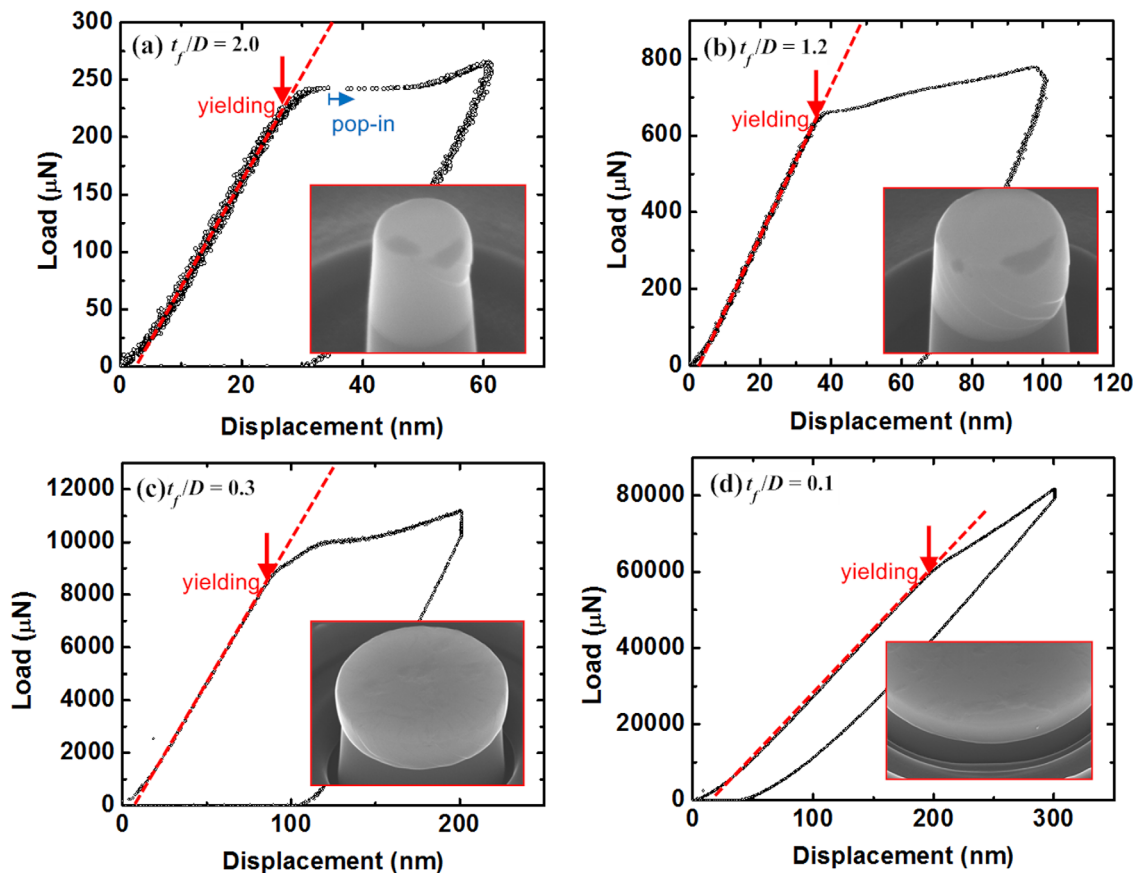


FIG. 6. (a)–(d) The typical load-displacement curves obtained from the microcompression of TFMG/Si composite micropillars with the same film thickness of 600 nm but different t_f/D ratios. Insets show the SEM micrographs of the corresponding micropillars after microcompression.

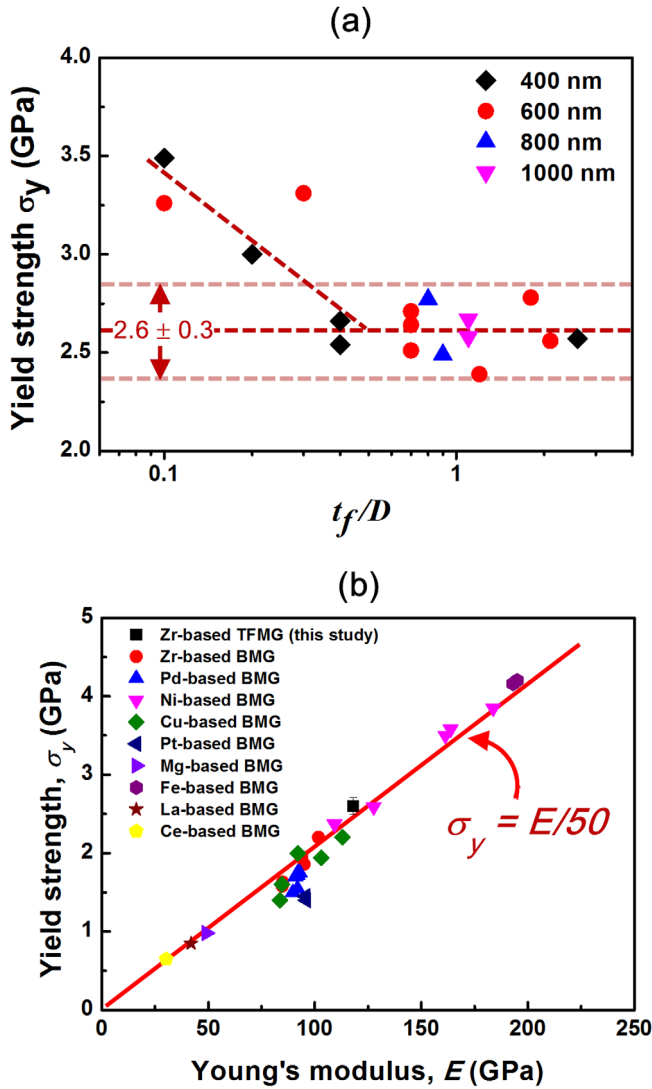


FIG. 7. (a) The variation of the yield strengths of the TFMGs obtained from micro-compression with their t_f/D ratios, and (b) the same trend of “strength-versus-modulus” correlation exhibited by the TFMG and BMGs. The data of BMGs are taken from Ref. 20.

can be translated into a fraction of the residual stress, σ_r by invoking a proper yielding criterion. In principle, one can select either the Mohr-Coulomb (MC) or Drucker-Prager (DP) model to estimate σ_r , both of which have been widely accepted as the yielding criterion for MGs in the MG literature.^{19,22–24} Here, both two are utilized for the sake of comparison. After the necessary derivations, one can readily obtain the following formulas:

$$\sigma_r = \frac{\sin \theta \cos \theta - \mu \sin^2 \theta}{\sin \theta \cos \theta + \mu \cos^2 \theta} (\sigma_y - \sigma_0), \quad (\text{MC Model}) \quad (1a)$$

$$\sigma_r = \frac{1 - f/3}{1 + f/3} (\sigma_y - \sigma_0), \quad (\text{DP Model}) \quad (1b)$$

where θ is the shear angle ($\sim 42^\circ$) in a MG sample under compression, μ is the so-called frictional coefficient (~ 0.1 for Zr-based MGs),¹⁹ and f is the parameter in the DP model accounting for the tension-compression asymmetry, which can be expressed as $f = 3 \frac{\sigma_c - \sigma_t}{\sigma_c + \sigma_t}$ and usually takes on the value

~ 0.13 for the Zr-based MGs. Here σ_c and σ_t denote the compressive and tensile yield strength of a MG, respectively. Note that when using Eq. (1a) or (1b) to compute the residual stress in a TFMG, both σ_y and σ_0 are taken to be positive. However, the calculated result of Eq. (1a) or (1b) could be negative if σ_r is compressive or positive if σ_r is tensile.

The calculated residual stresses σ_r , ranging from ~ 0.6 GPa to ~ 0.8 GPa, are tabulated in Table I, from which no discernable thickness effect can be found. By switching from one yielding model to the other, we found that the calculated σ_r only differs by $\sim 10\%$, indicative of the robustness of the current method. Unlike the compressive residual stress previously reported for the TFMGs,¹³ which originates from the structural mismatch between the film and substrate, however, the tensile residual stress here obtained is essentially a thermo-stress, which can be justified as follows. According to Kato and co-workers,²⁵ the Zr-Cu-Al-Ni BMG possesses a RT thermal expansion coefficient, α_{MG} , of $11.3 \times 10^{-6} \text{ K}^{-1}$, which is about two times that of the Si substrate ($\alpha_{\text{Si}} = 6 \times 10^{-6} \text{ K}^{-1}$). Assuming that the TFMGs possess a similar thermal expansion coefficient, we can thus foresee a tensile residual stress developed in the TFMGs after the chamber temperature drops from 80°C to RT. According to Ref. 26, the thermo-stress can be expressed as $\sigma_r \sim E_f \Delta T \Delta \alpha / (1 - \nu)$, where $E_f \sim 100$ GPa, $\nu = 0.36$, $\Delta T = 50$ K and $\Delta \alpha = \alpha_{\text{MG}} - \alpha_{\text{Si}} \sim 5 \times 10^{-6} \text{ K}^{-1}$. As a result, the thermo-stress on the order of 0.1 GPa in the TFMGs can be estimated, which agrees with our previous calculation.

B. Substrate effect and hydrostatic pressure

At the macroscopic scale, a geometric constraint hinders shear-band propagation in BMGs, thus improving their plasticity through shear-band multiplication.²⁷ Here, we further show that the existence of a geometric constraint at the nano-scale, like the bonded TFMG/Si interface, may even help to suppress shear-band nucleation through the development of a large hydrostatic pressure in the thin film.

As the TFMGs are pressed against their underlying substrate, a hydrostatic pressure builds up with its magnitude varying with the t_f/D ratio. To gain a quantitative insight into the variation of such a hydrostatic pressure, we performed a finite-element (FE) analysis of the elastically deformed TFMGs. Assuming an intact TFMG/Si interface, we can simplify the FE analysis by having the upper surface of the TFMG as a free end while the lower surface as a fixed end. Furthermore, the diamond punch was taken to be rigid when in contact with the TFMG. Figures 8(a)–8(d) display the

TABLE I. The estimated tensile residual stress in the TFMGs. Note that $\theta = 42^\circ$, $\mu = 0.1$, and $f = 0.13$ are used in calculation.

t_f (nm)	σ_y (GPa)	$\sigma_0 (=H_f/3)$ (GPa)	σ_r (GPa)	
			DP model	MC model
400	2.6	1.87	0.67	0.60
600	2.6	1.90	0.64	0.57
800	2.6	1.73	0.80	0.71
1000	2.6	1.80	0.73	0.66

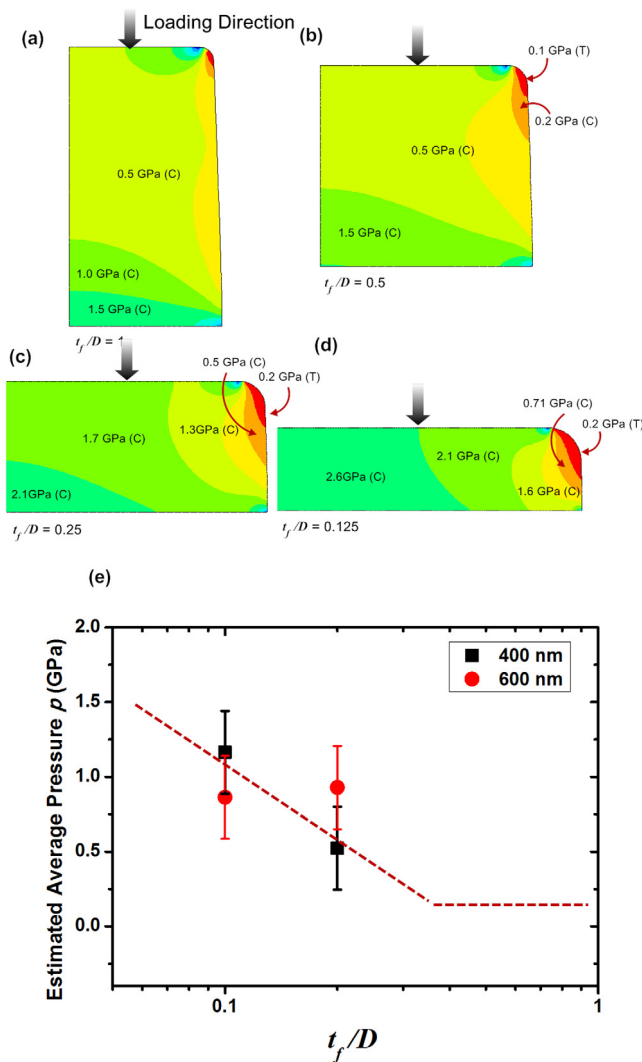


FIG. 8. The contour plots for the distribution of hydrostatic pressure corresponding to an elastic strain of 2% in the TFMGs with the t_f/D ratios of (a) 1.0, (b) 0.5, (c) 0.25, and (d) 0.125, and (e) the average hydrostatic pressure estimated in the TFMGs with the t_f/D ratio less than 0.3.

simulated distribution of the hydrostatic pressure in the TFMGs at four different t_f/D ratios (1, 0.5, 0.25, and 0.125) at the same elastic strain of $\sim 2\%$. To mimic the real experimental set-up, the FE models of the TFMGs are all tapered with a taper angle of $\sim 3^\circ$ and slight tip rounding. Conforming to our expectation, a large high hydrostatic pressure is observed at the TFMG/Si interface, spreading out to the bulk of the TFMG. With the t_f/D ratio decreasing from 1 to 0.125, the average hydrostatic pressure is elevated from ~ 0.5 GPa to ~ 2 GPa. To a certain extent, these numerical results explain the rising trend of the yield strengths measured in microcompression, as seen in Fig. 7(a). By using the DP model, we can extract the average hydrostatic pressure in the TFMGs, which was done by taking $\sigma_y = 2.6 \pm 0.3$ GPa as the intrinsic yield strength free of the substrate effect. In such a case, the hydrostatic pressure p exerted by the Si substrate can be simply expressed as $p = \frac{3-f}{f}(\sigma_l - \sigma_y)$, where σ_l denotes the substrate-affected yield strength. As seen in Fig. 8(e), the estimated hydrostatic pressure p emerging at the yielding point of the TFMG increases from ~ 0.5 to ~ 1 GPa as the t_f/D ratio of the micropillar decreases from ~ 0.2 to ~ 0.1 .

C. Transition of plastic deformation mode

From the viewpoint of the free-volume model,²⁸ a large hydrostatic pressure can delay shear-band nucleation instability, thus increasing the critical length of a bona fide shear band. This can be simply pictured as a “pressure-caging” effect. As a hydrostatic pressure tends to squeeze atoms and their neighbors into a more closely packed environment, it becomes harder to shear the atoms for creating a dilated shear-banding region in the presence of a large hydrostatic pressure than otherwise. This is similar to the nucleation of a frictional shear crack in an elastic body. By increasing the pressure normal to the sites abundant in micro-cracks, the frictional force acts to stabilize their sub-critical growth, hence resulting in a longer critical crack length before instability occurs.²⁹ However, this “pressure-caging” effect is hard to witness in a bulk sample as the sample size is of several orders of magnitude larger than the critical shear-band nucleation length, which is thought to be about ~ 100 nm according

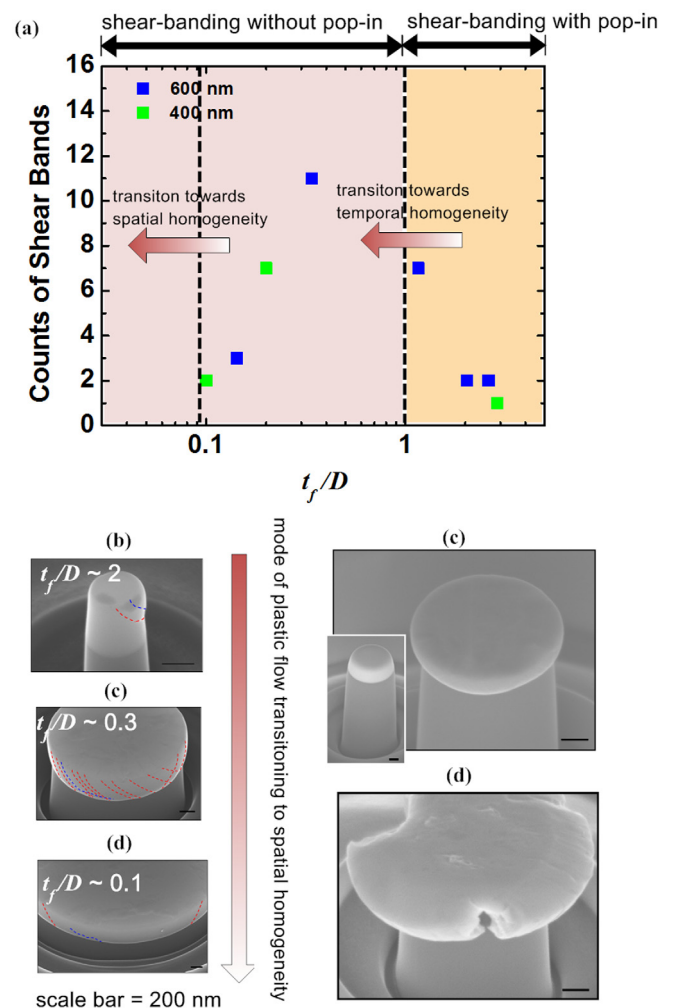


FIG. 9. (a) The variation of the number of shear bands with the t_f/D ratio which are observable on the 400-nm and 600-nm thick TFMG/Si micropillars deformed to the same plastic strain of $\sim 10\%$, (b)-(c) the shear-banding traces (as marked by the dotted curves) observed on the 600-nm thick TFMG/Si micropillars deformed to the same plastic strain as in (a), (c) the absence of shear-banding traces on the 400-nm thick TFMG/Si micropillar when plastically deformed by 20% (the inset shows the micropillar prior to microcompression), and (d) the peculiar mushroom-like morphology of a 600-nm thick TFMG/Si micropillar after severe plastic deformation.

to the previous nano-tension results.^{3,4} In our current micro-compression tests, we are curious about if the “pressure-caging” effect can be observed or not in the thin films.

To verify the above idea, we compressed a series of 400-nm and 600-nm thick TFMGs with different t_f/D ratios to the same plastic strain of 5%. From the obtained load-displacement curves, we did not see any displacement discontinuity or pop-in. However, the deformed TFMGs still show a population of shear traces on their other surface. Figure 9(a) displays the variation of the number of the observable shear traces with the t_f/D ratio. Note that all SEM observations were made at the same condition when the shear traces were counted. From Fig. 9(a), it can be seen that the number of the shear traces grows rapidly with the decreasing t_f/D ratio for $t_f/D > 0.3$. This phenomenon can be confirmed with the SEM micrographs, as shown in Figs. 9(b) and 9(c), which is analogous to multiple shear-banding in a deformed BMG sample geometrically confined. Interestingly, this trend is reversed as the t_f/D ratio is further reduced (Figs. 9(a) and 9(c)). Since shear banding is identified by deformation localization, the paucity of shear traces implies that the plastic flow tends to transit into a spatially homogeneous plastic flow in the presence of a large hydrostatic pressure. This phenomenon of deformation mode transition can be more easily perceived when the t_f/D ratio of the TFMGs is dramatically reduced at large plastic deformations. As shown in Fig. 9(e), a 400-nm TFMG with the original $t_f/D \sim 0.2$ was deformed to a plastic strain of $\sim 20\%$, which exhibits a barrel-like morphology without any apparent shear traces. More dramatically, the TFMGs could be even pressed into a “mushroom” shape

without deformation localization (Fig. 9(f)). All these phenomena indicate that the TFMGs are extremely malleable and shear-banding diminishes when the combined substrate-and-size effect prevails.

Before concluding, we would like to present a TEM observation of the structural change in the vicinity of the TFMG/Si interface after severe plastic deformation, where a high strain concentration can be anticipated. Figure 10(a) displays a typical TEM micrograph of the deformed structure near the TFMG/Si interface. As shown in Fig. 10(b), the TFMG still retain its amorphous structure without an apparent structural change, such as nanocrystallization, in the region a few nanometers away from the interface; in contrast, a few stacking faults were observed in the Si (Figs. 10(a) and 10(c)). In the vicinity of the triple junction among the Si substrate, the interface and the TFMG, local structural ordering can be found at the TFMG side (Fig. 10(c) and the inset). By comparison, the Si substrate exhibits a nearly perfect or unfaulted crystalline structure in its bulk, which conforms to the notion that the Si substrate in general deforms only in an elastic fashion (Fig. 10(d)).

V. CONCLUDING REMARKS

In conclusion, we have performed a systematic study on the mechanical behavior of the Zr-based TFMGs at RT. Compared to the previous work on TFMGs,^{9,13,15,17,30,31} salient conclusions can be drawn below:

- (1) When bonded onto the Si substrate, the Zr-based TFMGs exhibit hardness significantly lower than their bulk counterparts, which is due to the tensile residual stress developed in the TFMGs.
- (2) The yield strengths of the TFMGs obtained from micro-compression are strongly dependent on the shape of the FIB-milled micropillars. This shape dependence is essentially a manifestation of the substrate effect and can be rationalized with the pressure-dependent yielding model.
- (3) Due to the combined substrate-and-size effect, the plastic flow in the TFMGs could transit smoothly from an inhomogeneous to homogeneous mode. Contrasting the conventional notion of the plastic deformation mode transition induced by size reduction, our work show that the homogenization of the plastic flow in the TFMGs can be triggered by the shape change in the TFMG-based micropillars for a same film thickness.

ACKNOWLEDGMENTS

Y.Y. acknowledges the financial support provided by the Research Grant Council (RGC), the government of the Hong Kong special administrative region (SAR), via the General Research Fund (GRF) with the account number PolyU 5327/10E and CityU 530711, while J.P.C. thanks the support (Grant No. NSC 98-2221-E-011-037-MY3) from National Science Council (NSC) of Taiwan, R.O.C.

¹M. F. Ashby and A. L. Greer, “Metallic glasses as structural materials,” *Scr. Mater.* **54**, 321–326 (2006).

²C. A. Schuh, T. C. Hufnagel, and U. Ramamurty, “Mechanical behavior of amorphous alloys,” *Acta Mater.* **55**(12), 4067–4109 (2007).

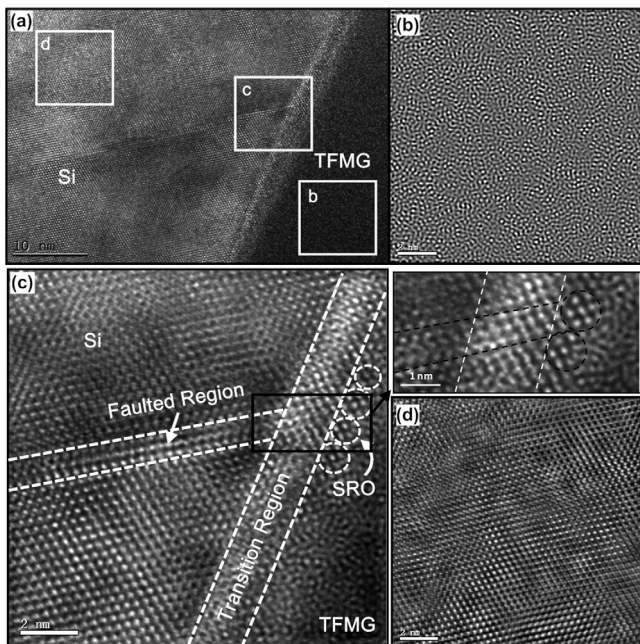


FIG. 10. (a) The HRTEM image of the TFMG/Si system after severe plastic deformation in microcompression, (b) the FFT-filtered image of the amorphous structure in the TFMG, (c) the FFT-filtered image showing the emission of partial dislocations with stacking faults from the TFMG/Si interface [inset highlights the faulted region in the Si connected with the short-range-order (SRO) region in the TFMG], and (d) the FFT-filtered image of the crystalline structure in the Si substrate.

- ³H. Guo, P. F. Yan, Y. B. Wang, J. Tan, Z. F. Zhang, M. L. Sui, and E. Ma, "Tensile ductility and necking of metallic glass," *Nature Mater.* **6**(10), 735–739 (2007).
- ⁴D. Jang and J. R. Greer, "Transition from a strong-yet-brittle to a stronger-and-ductile state by size reduction of metallic glasses," *Nature Mater.* **9**(3), 215–219 (2010).
- ⁵J. C. Ye, J. Lu, Y. Yang, and P. K. Liaw, "Study of the intrinsic ductile to brittle transition mechanism of metallic glasses," *Acta Mater.* **57**(20), 6037–6046 (2009).
- ⁶Y. Yang, J. C. Ye, J. Lu, P. K. Liaw, and C. T. Liu, "Characteristic length scales governing plasticity/brittleness of bulk metallic glasses at ambient temperature," *Appl. Phys. Lett.* **96**(1), 011905 (2010).
- ⁷Y. Yang and C. T. Liu, "Size effect on stability of shear band propagation in bulk metallic glasses: An overview," *J. Mater. Sci.* **47**, 55–67 (2012).
- ⁸Y. Yang, J. C. Ye, J. Lu, Y. F. Gao, and P. K. Liaw, "Metallic glasses: Gaining plasticity for microsystems," *JOM-US* **62**(2), 93–98 (2010).
- ⁹J. P. Chu, J. C. Huang, J. S. C. Jang, Y. C. Wang, and P. K. Liaw, "Thin film metallic glasses: preparations, properties, and applications," *JOM* **62**(4), 19–24 (2010).
- ¹⁰S. Hata, J. Sakurai, and A. Shimokohbe, in *18th IEEE international conference on MEMS 2005* (2005), pp. 479–482.
- ¹¹Y. Yang, J. C. Ye, J. Lu, F. X. Liu, and P. K. Liaw, "Effects of specimen geometry and base material on the mechanical behavior of focused-ion-beam-fabricated metallic-glass micropillars," *Acta Mater.* **57**, 1613–1623 (2009).
- ¹²W. C. Oliver and G. M. Pharr, "An improved technique for determining hardness and elastic modulus using load and displacement sensing indentation experiments," *J. Mater. Res.* **7**, 1564 (1992).
- ¹³J. P. Chu, J. S. C. Jang, J. C. Huang, H. S. Chou, Y. Yang, J. C. Ye, Y. C. Wang, J. W. Lee, F. X. Liu, Y. F. Gao, P. K. Liaw, Y. C. Chen, C. M. Lee, C. L. Li, and C. Rullynai, "Thin film metallic glasses: Unique properties and potential applications," *Thin Solid Films* **520**(16), 5097–5122 (2012).
- ¹⁴R. Saha and W. D. Nix, "Effects of the substrate on the determination of thin film mechanical properties by nanoindentation," *Acta Mater.* **50**, 23 (2002).
- ¹⁵H. S. Chou, J. C. Huang, L. W. Chang, and T. G. Nieh, "Structural relaxation and nanoindentation response in Zr-Cu-Ti amorphous thin films," *Appl. Phys. Lett.* **93**, 191901 (2008).
- ¹⁶M. C. Liu, C. J. Lee, Y. H. Lai, and J. C. Huang, "Microscale deformation behavior of amorphous/nanocrystalline multilayered pillars," *Thin Solid Films* **518**, 7295 (2010).
- ¹⁷H. S. Chou, J. C. Huang, and L. W. Chang, "Mechanical properties of ZrCuTi thin film metallic glass with high content of immiscible tantalum," *Surf. Coat. Technol.* **205**, 587 (2010).
- ¹⁸A. Inoue, "Stabilization of metallic supercooled liquid and bulk amorphous alloys," *Acta Mater.* **48**, 279 (2000).
- ¹⁹J. C. Ye, J. Lu, Y. Yang, and P. K. Liaw, "Extraction of bulk metallic-glass yield strengths using tapered micropillars in micro-compression experiments," *Intermetallics* **18**(3), 385–393 (2010).
- ²⁰W. L. Johnson and K. Samwer, "A universal criterion for plastic yielding of metallic glasses with a $(T/T_g)^{2/3}$ temperature dependence," *Phys. Rev. Lett.* **95**(19), 195501 (2005).
- ²¹M. D. Uchic, P. A. Shade, and D. M. Dimiduk, "Plasticity of micrometer-scale single crystals in compression," *Annu. Rev. Mater. Res.* **39**, 361–386 (2009).
- ²²C. H. Hsueh, H. Bei, C. T. Liu, E. P. George, and P. F. Becher, "Controlled normal/shear loading and shear fracture in bulk metallic glasses," *Intermetallics* **17**, 802–810 (2009).
- ²³C. A. Schuh and A. C. Lund, "Atomistic basis for the plastic yield criterion of metallic glass," *Nature Mater.* **2**, 449–452 (2003).
- ²⁴M. Zhao and M. Li, "A constitutive theory and modeling on deviation of shear band inclination angles in bulk metallic glasses," *J. Mater. Res.* **24**(8), 2688–2696 (2009).
- ²⁵H. Kato, H.-S. Chen, and A. Inoue, "Relationship between thermal expansion coefficient and glass transition temperature in metallic glasses," *Scr. Mater.* **58**, 1106–1109 (2008).
- ²⁶L. B. Freund and S. Suresh, *Thin Film Materials: Stress, Defect Formation and Surface Evolution* (Cambridge University Press, 2003).
- ²⁷Z. F. Zhang, H. Zhang, X. F. Pan, J. Das, and J. Eckert, "Effect of aspect ratio on the compressive deformation and fracture behaviour of Zr-based bulk metallic glass," *Philos. Mag. Lett.* **85**(10), 513–521 (2005).
- ²⁸F. Spaepen, "A microscopic mechanism for steady state inhomogeneous flow in metallic glasses," *Acta Metall.* **25**(4), 407–415 (1977).
- ²⁹Q. H. Zuo and J. K. Dienes, "On the stability of penny-shaped cracks with friction: the five types of brittle behavior," *Int. J. Solids Struct.* **42**, 1309–1326 (2005).
- ³⁰C. L. Chiang, J.P. Chu, F. X. Liu, P. K. Liaw, and R. A. Buchanan, "A 200 nm thick glass-forming metallic film for fatigue-property enhancements," *Appl. Phys. Lett.* **88**, 131902 (2006).
- ³¹A. Donohue, F. Spaepen, R. G. Hoagland, and A. Misra, "Suppression of the shear band instability during plastic flow of nanometer-scale confined metallic glasses," *Appl. Phys. Lett.* **91**(24), 241905 (2007).